

The Study of Mass Distribution of products in 7.0 AMeV $^{238}\text{U}+^{238}\text{U}$ Collisions

Kai Zhao,¹ Xizhen Wu,^{1,*} and Zhuxia Li^{1,2,†}

¹*China Institute of Atomic Energy,
P.O. Box 275(18), Beijing 102413, P. R. China*

²*Institute of Theoretical Physics, Chinese Academic of Science, Beijing 100080, P. R. China*

(Dated: April 17, 2019)

Abstract

Within the Improved Quantum Molecular Dynamics (ImQMD) Model incorporating the statistical decay Model, the reactions of $^{238}\text{U}+^{238}\text{U}$ at the energy of 7.0 AMeV have been studied. The charge, mass and excitation energy distributions of primary fragments are investigated within the ImQMD model and de-excitation processes of those primary fragments are described by the statistical decay model. The mass distribution of the final products in $^{238}\text{U}+^{238}\text{U}$ collisions is obtained and compared with the recent experimental data.

*Electronic address: lizwux9@ciae.ac.cn

†Electronic address: lizwux@ciae.ac.cn

I. Introduction

When beams in the actinide region with bombarding energies above the Coulomb barrier became available about twenty years ago, the strongly damped reactions in very heavy systems, such as in $^{238}\text{U} + ^{238}\text{U}$ were studied[1, 2, 3]. These early experiments emphasized the investigation on the decay channels of the di-nuclear system (for production of super-heavy nuclei) or on particle creation in the strong electromagnetic fields. Recently, renewed interest in this subject has been motivated by the necessity of clarifying the dynamics of very heavy nuclear collisions at low excitation energies and by the search for new ways of producing neutron-rich superheavy nuclei. Based on coupled Langevin-type equations, a model for the simultaneous description of deep inelastic scattering, quasi-fission, fusion and regular fission was proposed in ref. [4]. Within this model the reactions of $^{238}\text{U}+^{238}\text{U}$, $^{232}\text{Th}+^{250}\text{Cf}$ and $^{238}\text{U}+^{248}\text{Cm}$ were investigated and a large transfer of charge and mass were found in those reactions as a result of an inverse quasi-fission process[4, 5]. Owing to very heavy nuclear system and very complicated process, a large number of degrees of freedom, such as the excitation and deformation of projectile and target, the neck formation, nucleon transfer, different types of separation of the composite system and nucleon emission will simultaneously play a role. Thus, one faces a difficulty for handling the problem with such complex mechanism and large number of degrees of freedom by the macroscopic dynamics model. In this case, a microscopic transport theory model is worthy to be used[6, 7]. In ref. [7] the formation and properties of the transiently formed composite systems in Strongly damped reactions of $^{238}\text{U}+^{238}\text{U}$, $^{232}\text{Th}+^{250}\text{Cf}$ at $E_{cm}=680-1880$ MeV were studied based on the ImQMD model. One found that the weakly repulsive entrance channel potential and strong dissipation delay the re-separation time of a composite system, and a 15-20 MeV high Coulomb barrier at the surface of the single-particle potential well of the composite system makes the excited unbound protons still embedded in the potential well and to move in a common mono-single-particle potential for a period of time. These two effects restrains the quick decay of the composite system. That study results in our interest for the incident-energy dependence of lifetime of the composite system. We found that the longest average lifetime for the composite system of $^{238}\text{U}+^{238}\text{U}$ could reach to over ~ 1000 fm/c at the incident energy region 1000 to 1300 MeV. Recent study on the incident-energy dependence of the lifetime of the transiently formed giant composite system $^{238}\text{U}+^{238}\text{U}$ by means of TDHF

calculations based on Skyrme energy density functional[8] confirmed this results. Since the correlation (fluctuation) effect is considered in the ImQMD model, it is able to calculate the mass (charge) distribution of primary fragments in the $^{238}\text{U}+^{238}\text{U}$ reaction, in addition to study the properties of the composite systems. The experiment for the reaction $^{238}\text{U}+^{238}\text{U}$ at energies close to the Coulomb barrier was performed at GANIL and the mass distributions of products for the reaction at several energies are available now[9, 10], which stimulates us to make further study of the decay of the composite system of $^{238}\text{U}+^{238}\text{U}$.

In this work. we study the mass distribution of products in $^{238}\text{U}+^{238}\text{U}$ at 7 AMeV and then compare it with the experimental data. Considering the extremely complexity of the reaction process and saving computation time, we describe the reaction process by a two step model, i.e. a dynamical reaction process described by the ImQMD model followed by a statistical decay process which is described by a statistical decay model.

The paper is organized as follows: In section II we will briefly introduce the theoretical models. In section III and IV we present the results of primary fragments and final products, respectively. Finally, we will give brief summary in section V.

II. Theoretical Model

Within this approach, the first step describes the formation and re-separation process of the transiently formed composite systems of $^{238}\text{U}+^{238}\text{U}$ by means of the ImQMD model. The primary fragments and fast particle emission are obtained at the end of ImQMD calculations. The second step devotes to describe the decay of the primary fragments by means of HIVAP incorporating with a three Gaussian model for describing the mass distribution of fission fragments. And finally the mass distribution of the products is obtained.

A. The ImQMD model

Detailed description of the ImQMD model and its applications in low energy heavy ion collisions can be found in Refs. [6, 7, 11, 12]. Here, we only mention that in this model the nuclear potential energy is an integration of the potential energy density functional which reads

$$V_{\text{loc}} = \frac{\alpha \rho^2}{2 \rho_0} + \frac{\beta}{\gamma + 1} \frac{\rho^{\gamma+1}}{\rho_0^\gamma} + \frac{g_0}{2\rho_0} (\nabla\rho)^2$$

$$+ \frac{c_s}{2\rho_0}(\rho^2 - \kappa_s(\nabla\rho)^2)\delta^2 + g_\tau \frac{\rho^{\eta+1}}{\rho_0^\eta}, \quad (1)$$

where ρ , ρ_n , ρ_p are the nucleon, neutron, and proton density, $\delta = (\rho_n - \rho_p)/(\rho_n + \rho_p)$ is the isospin asymmetry. The parameters in above expressions are given in the table I[6].

$\alpha(\text{MeV})$	$\beta(\text{MeV})$	γ	$g_0(\text{MeV}fm^2)$	$g_\tau(\text{MeV})$	η	$c_s(\text{MeV})$	$\kappa_s(fm^2)$	$\rho_0(fm^{-3})$
-356	303	7/6	7.0	12.5	2/3	32	0.08	0.165

TABLE I: the model parameters

The Coulomb energy is also included in the Hamiltonian written as a sum of the direct and the exchange contribution:

$$U_{Coul} = \frac{1}{2} \int \int \rho_p(\mathbf{r}) \frac{e^2}{|\mathbf{r} - \mathbf{r}'|} \rho_p(\mathbf{r}') d\mathbf{r} d\mathbf{r}' - e^2 \frac{3}{4} \left(\frac{3}{\pi} \right)^{1/3} \int \rho_p^{4/3} d\mathbf{R}. \quad (2)$$

In the collision term, isospin-dependent nucleon-nucleon scattering cross sections[13] are used and the Pauli blocking effect is treated more strictly[14, 15].

It is of crucial importance to make the initial nuclei in the real ground state because considerable excitation of initial nuclei will produce unreal particle emission and the residue with too high excitation which will completely masks the real decay process of residue. We check carefully not only the binding energy and the root-mean-square radius of the initial nuclei but also their time evolution. The average binding energy per nucleon of initial nuclei is required to be $E_{g.s.} \pm 0.1$ MeV, where $E_{g.s.}$ is the binding energy of nuclei in ground state. It is required that those initial nuclei with no spurious particle emission and their properties such as binding energy and root-mean-square radius being stable within 6000fm/c are taken to be as good initial nuclei, and then are applied in the simulation of reaction process. The deformation of the initial ^{238}U ($\varepsilon=0.24$) is considered in the initial condition. In the simulation of reactions, the initial orientations of two deformed ^{238}U are randomly taken. Fig.1 shows the time evolution of the binding energy and root-mean-square radius of the initial ^{238}U .

At the end of the ImQMD calculations, fragments are constructed by means of the coalescence model widely used in the QMD calculations. In this work only the primary fragments with mass number larger than 50 are considered. Then, we calculate the total energy of

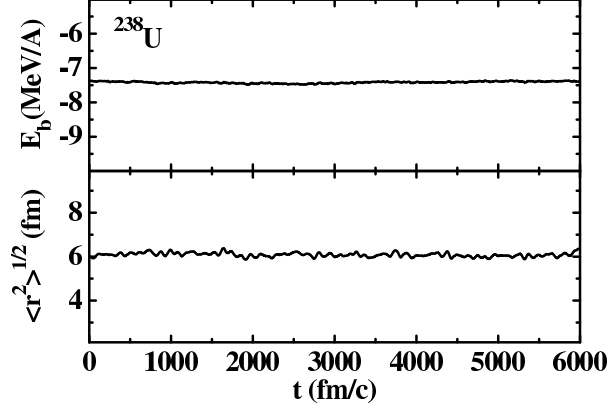


FIG. 1: The time evolution of the binding energy and root-mean-square radius of the initial ^{238}U .

each excited fragment in its rest frame and its excitation energy is obtained by subtracting the corresponding ground state energy from the total energy of the excited fragment.

B. The statistical decay model

The second step describes the decay process of primary fragments by emission of neutron, proton and α particle and fission. The statistical decay model (HIVAP code)[16] incorporating a 3-Gaussian model for mass distribution of fission fragments for fissile nuclei is used to describe the decay process of primary fragments and mass distribution of final products. In HIVAP, the survival probability of an excited primary fragment is given by subsequent de-excitation process leading to a given final evaporation-residue nucleus in its ground state. Successive stages of a subsequent de-excitation processes for primary fragment with mass A , charge Z and excitation energy E are determined by branching ratios expressed by relative partial decay widths for all possible decay modes, $\Gamma_i(A, Z, E)/\Gamma_{tot}(A, Z, E)$, where $i=n,p,d,\alpha$, etc., and $\Gamma_{tot}(A, Z, E)$ is the sum of all particle decay widths $\Gamma_i(A, Z, E)$ and the fission width $\Gamma_f(A, Z, E)$. All partial widths for emission of light particles and fission for excited nuclei are calculated by the HIVAP code.

The excited actinide and transactinide nuclei in primary fragments and those produced in the de-excitation process undergo a fission. The production probability of a fission fragment with mass number A_1 is calculated as follows:

$$W_f(A_1) = \sum_{A,Z,E} \frac{\Gamma_f(A, Z, E)}{\Gamma_{tot}(A, Z, E)} P(A_1, A, Z, E). \quad (3)$$

Where the $P(A_1, A, Z, E)$ is the production probability of a fragment with mass number A_1

from a fission of the excited nucleus with mass A , charge Z and excitation energy E . The $P(A_1, A, Z, E)$ is calculated based on an empirical three gaussian model. It reads

$$P(A_1, A, Z, E) = \sum_{j=1}^3 g^{(j)}(A_1, A, Z, E) \quad (4)$$

and

$$g^{(j)}(A_1, A, Z, E) = \frac{P^{(j)}(A, Z, E)}{\sqrt{2\pi}\sigma^{(j)}(A, Z, E)} \exp\left[-\frac{(A_1 - A^{(j)}(A, Z, E))^2}{2(\sigma^{(j)}(A, Z, E))^2}\right], \quad (5)$$

$$j=1,2,3.$$

Where, the Gaussian distribution $g^{(j)}(A_1, A, Z, E)$ represents one of the components of the mass distribution of fission. Among them, the $g^{(1)}(A_1, A, Z, E)$ and $g^{(2)}(A_1, A, Z, E)$ describe the asymmetric component of the mass distribution, and $g^{(3)}(A_1, A, Z, E)$ is for the symmetric component. $P^{(j)}(A, Z, E)$, $\sigma^{(j)}(A, Z, E)$ and $A^{(j)}(A, Z, E)$ are the parameters for 3 Gaussian distributions, which are the function of mass number A , charge Z and excitation energy E of fissile nucleus. The $P^{(j)}(A, Z, E)$ and $A^{(j)}(A, Z, E)$ obey the following relations

$$P^{(1)}(A, Z, E) = (1 - P^{(3)}(A, Z, E))\eta \quad (6)$$

$$P^{(2)}(A, Z, E) = (1 - P^{(3)}(A, Z, E))(1 - \eta) \quad (7)$$

$$A^{(1)}(A, Z, E) + A^{(2)}(A, Z, E) = A \quad (8)$$

$$A^{(3)}(A, Z, E) = \frac{A}{2} \quad (9)$$

Thus, only six parameters of $P^{(3)}(A, Z, E)$, η , $A^{(1)}(A, Z, E)$ and $\sigma^{(i)}(i=1,2,3)$ are independent, which need to be fixed according to available experimental data of fission mass distributions in actinide and transactinide nuclei.

For fitting the parameters in the three Gaussian empirical formula we collect available experimental data of fission mass distributions[17, 18, 19, 20, 21] as many as possible. For the case of lack of experimental data the interpolation or extrapolation method is employed. For ^{238}U , data for mass distributions of fission fragments at different energies are available so we can obtain the energy dependence of mass distribution of fission fragments through interpolation. But for other fissile nuclei those data are relatively lack. For these nuclei we suppose that they have similar energy dependence behavior with those of ^{238}U because the corresponding theoretical study is also lack for these nuclei. This, of course, will introduce

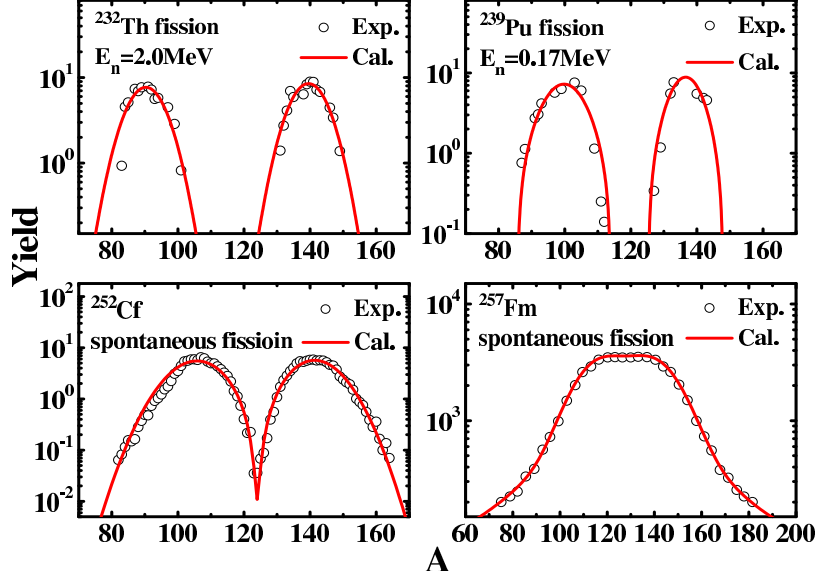


FIG. 2: (Color online) The mass distributions of fission for ^{232}Th , ^{239}Pu , ^{252}Cf and ^{257}Fm . The experimental data are taken from [21, 22, 23, 24]

a considerable approximation. However, in the reaction considered in this work, the fission for excited ^{238}U is the most important one among all fissile nuclei and we expect the approximation introduced in the energy dependence of the mass distribution of fission fragments will not destroy the final results. In Fig.2 and Fig.3 we show some examples of calculated mass distributions of fission for different nuclei and for different excitation energies and make comparison with experimental data. The curves and dots are for calculated results and data, respectively. From the figures we can see that the empirical formula seems to be able to reproduce the available experimental data and able to be used to calculate the mass distributions of actinide and transactinide fragments.

In order to choose matching time t_S of two models properly, we investigate the decay process of the transiently formed composite systems of $^{238}\text{U}+^{238}\text{U}$ at the energy of 7.0 AMeV. Fig.4 shows the time dependence of the surviving probability of fragments with $Z \geq 110$. One can see from the figure that at about $t=500\text{fm}/c$, two nuclei reach a touching configuration. After about $1000\text{fm}/c$ the composite system begins to re-separate with a very large decay rate and at about $3000\text{fm}/c$ almost all composite systems are separated. This process is described by the ImQMD model. The separated fragments continue to decay with a much smaller decay rate. This process is expected to be described by the statistical decay model. Thus, we select the matching time of two models to be $3000\text{fm}/c$. We have also

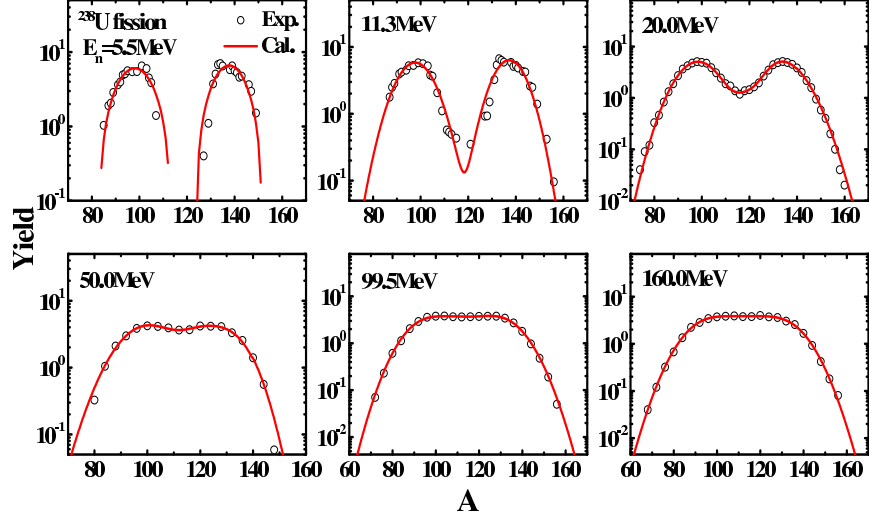


FIG. 3: (Color online) The mass distributions of fission for ^{238}U at different excitation energies. The experimental data are taken from [21]

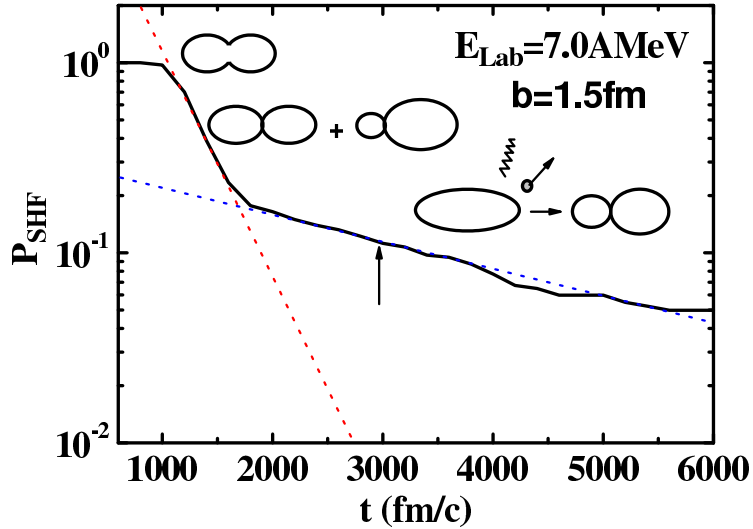


FIG. 4: (Color online) The time dependence of the surviving probability of super-heavy fragments of $Z > 110$.

tried other choices such as $t_S = 4000\text{fm}/c$, $5000\text{fm}/c$ and $6000\text{fm}/c$ and we find there is no change of final results. In the ImQMD calculations, 500 events per impact parameter are performed.

III. The Distribution of Mass, Charge and Excitation Energy in Primary Fragments

In order to study the final mass distribution of the reaction $^{238}\text{U} + ^{238}\text{U}$, we first study the distribution of primary fragments which are given at the end of ImQMD calculations.

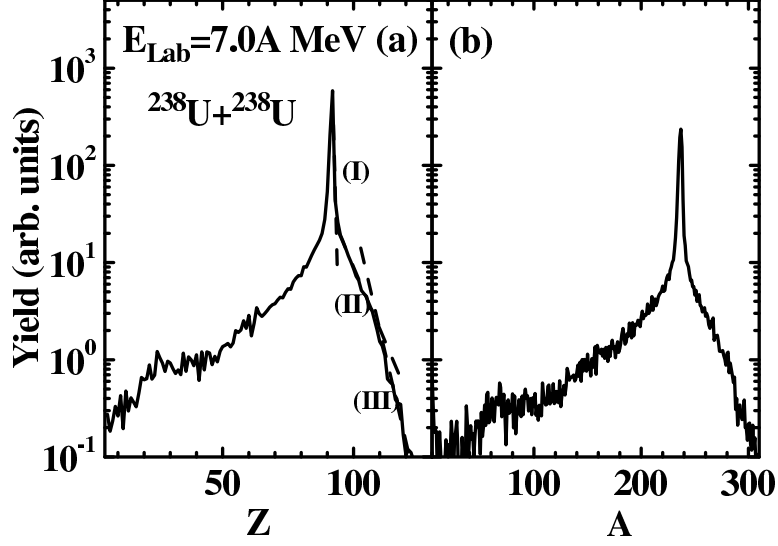


FIG. 5: (a)The charge and (b)the mass distribution of the primary fragments of $^{238}\text{U} + ^{238}\text{U}$ at 7.0A MeV.

The charge, mass and excitation energy distributions as well as the angular distribution of primary fragments are obtained by the ImQMD model calculations at time $t=3000\text{fm}/c$. The double differential cross section of a primary fragment with charge Z , mass A , excitation energy E and scattering angle θ is given by:

$$\frac{d^2\sigma_{pri}(Z, A, E, \theta)}{d\theta dE} = \int_0^{b_{max}} 2\pi b f(Z, A, E, \theta, b) db = \sum_{i=1}^{i_{max}} 2\pi b_i \Delta b f_i(Z, A, E, \theta, b_i), \quad (10)$$

where $f_i(A, Z, E, \theta, b_i)$ is the probability of producing the primary fragments with charge Z , mass A , excitation energy E and scattering angle θ under impact parameter b_i . The maximum impact parameter b_{max} is taken to be 14fm since there are no inelastic scattering when $b > 14\text{fm}$. The double differential cross section for primary fragments will be used as input in the second step for the calculations of final products in order to compare with the measurement. Let us first study the charge and mass distribution of primary fragments which is the integration of double differential cross sections. Fig.5 (a) and (b) show the charge and mass distribution of primary fragments ($A \geq 50$) for $^{238}\text{U} + ^{238}\text{U}$ at 7.0 A MeV, respectively. The sharp peak are located at the uranium for both subfigures. The primary fragments at the left side of the sharp peak stem from the re-separation of the composite system and fast fission products of actinide and transactinide fragments. The products at the right side of the sharp peak correspond to transuranium nuclei. The mass distributions of primary fragments at different impact parameter b are calculated in order to clarify the origin of the fragments

with different mass region. The results are shown in Fig.6. Subfigure (a), (b), (c) and (d) are for the impact parameter 0-4, 5-7, 8-10 and 11-14 fm, respectively. In central collisions (see subfig.6(a)) the mass number distribution of primary fragments extends to $A=320$ with a big asymmetric bump around $A=200-260$, which means a large mass transfer between two uranium nuclei happening in central collisions. At semi-central collision (subfig.6(b)), the mass distribution becomes less wide with a much shorter tail at right hand side. There are two peaks appeared in the mass distribution with bigger one corresponding to uranium and the smaller one originating from ternary fission(occasionally from quaternary-fission)events in reaction $^{238}\text{U}+^{238}\text{U}$. Clearly, in this case, very deep inelastic reaction becomes the most important reaction mechanism. For the peripheral collisions (subfig.6(c) and (d)) the mass distribution of primary fragments shows a symmetric peak with a very less variance. The reaction mechanism for peripheral reactions are of the inelastic or elastic scattering between two uranium nuclei. In order to understand the reaction mechanism and the mass distribution of fragments evolving with impact parameters shown in Fig.6 we present the average life-time of transiently formed composite system for $^{238}\text{U}+^{238}\text{U}$ at 7AMeV as function of impact parameter in Fig.7. From this figure, one can see that the life- time of composite system increases as impact parameter decreases. In the central collisions, two uranium nuclei have longer interaction time, stronger dissipation of collective motion and thus have stronger mass transfer between them compared with larger impact parameter cases. Therefore, the transuranium primary fragments mainly come from the central and semi-central collisions. Now we study the distribution of excitation energies of excited fragments. Fig.8 and Fig.9 show the excitation energy distributions for fragments with $Z \geq 100$ and $90 \leq Z \leq 94$, respectively. As is mentioned above that the fragments with $Z \geq 100$ come from the large mass transfer reactions which only happen in the central and semi-central collisions, the results shown in Fig.8 are only for impact parameter $b=0-4$ and $5-7$ fm. Fig.9 shows the results from deep inelastic scattering of $^{238}\text{U}+^{238}\text{U}$. One sees from both Fig.8(a) and Fig.9(a) that the primary fragments produced in central collisions are mostly highly excited and for those fragments the survival probability should be very low but still there is a tail extending to low exciting energy, which may have certain but very small survival probability. Whereas for the semi-central collision (see Fig.8(b) and Fig.9(b)) the high excitation energy primary fragments decreases and the portion of low energy primary fragments increases, thus, it is expected that some of fragments with $Z \geq 92$ can be survival. In the peripheral collisions (

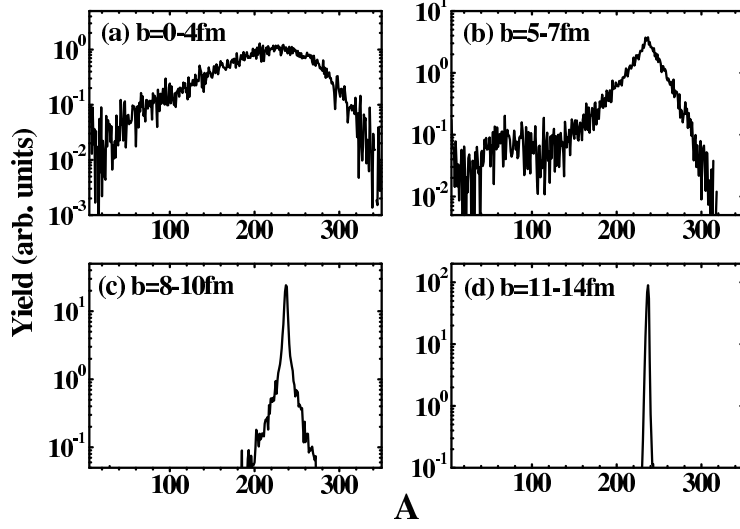


FIG. 6: The mass distributions of the primary fragments at different impact parameter regions.

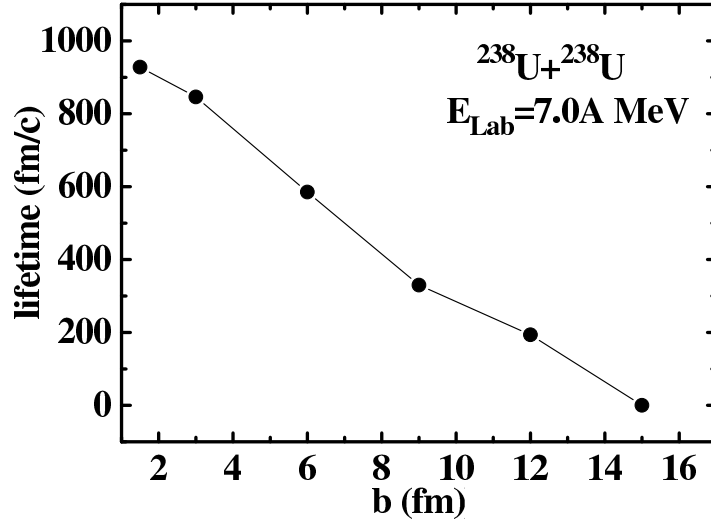


FIG. 7: The impact parameter dependence of the average life-time for the composite system of $^{238}\text{U}+^{238}\text{U}$ at 7 AMeV

see Fig.9(c) and (d))the excitation energies of primary fragments are much lower compared with the central and semi-central cases and the reason for it is of understandable.

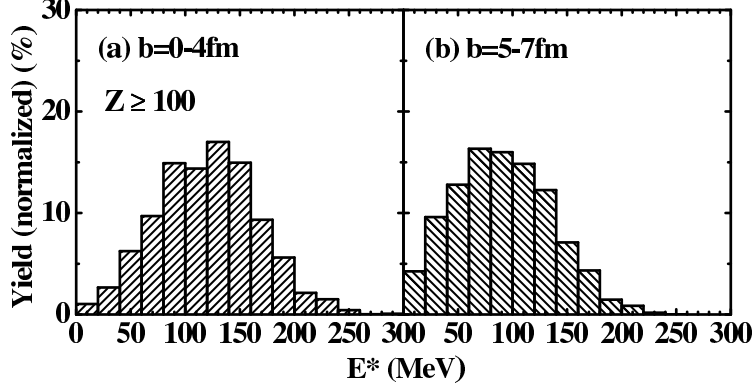


FIG. 8: The excitation energy distribution of the transuranic fragments with $Z \geq 100$ under condition of impact parameters (a) $b \leq 4$ fm and (b) $b = 5-7$ fm, respectively.

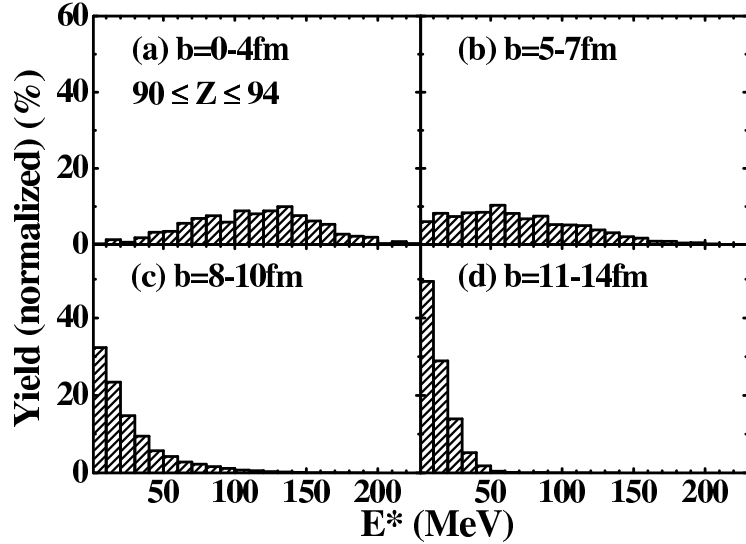


FIG. 9: The excitation energy distribution of the primary fragments around uranium ($90 \leq Z \leq 94$) for impact parameters (a) $b \leq 4$ fm, (b) $b = 5-7$ fm, (c) $b = 8-10$ fm and (d) $b = 11-13$ fm, respectively.

IV. Mass Distribution of Final Products

From the ImQMD model calculation we obtain the distributions of charges, masses and excitation energies for all produced primary fragments in $^{238}\text{U} + ^{238}\text{U}$ collisions. These primary fragments will de-excite through emitting light particles, γ -rays and fission. The decay process and the final products are described by the statistical evaporation model (HIVAP code) incorporated the three Gaussian fission model described in Section II. Based on the model, the mass distribution of final products for $^{238}\text{U} + ^{238}\text{U}$ at the incident energy of 7.0 AMeV can be calculated. In Fig.10, we show the calculated results of final products at 4 impact parameter regions of 0-4, 5-7, 8-10 and 11-14 fm. For central collisions(see Fig.10(a)), the

re-separation primary fragments of $^{238}\text{U}+^{238}\text{U}$ systems carry high excitation energies, the most part of them undergoes symmetric fission and thus a single bump of mass yield is found at around mass number 120. The rest of fragments not undergoing fission will evaporate particles and their residues finally form a shoulder in the mass distribution around Pb, which is due to strong shell effect for those nuclei around Pb. The yields for transuranic fragments decrease rapidly as mass increase, which is due to the high excitation energy of primary fragments in central collisions as seen from Fig.8(a). Here we should mention that the yields of the transuranic nuclei is not so certain because the fission barrier and the fission width for super-heavy nuclei and the transuranic nuclei are largely uncertain. For semi-central collisions, i.e. in the impact parameter region of 5-7 fm (see Fig.10(b)), the excitation energies carried by primary fragments are much less than those in the central collisions, so there appears a broad bump at mass number region of $80 \leq A \leq 170$ which is the superposition of symmetric and asymmetric fission. There appears another small bump centered at Uranium ($A \approx 230$). The shallow valley between two bumps means that the yields of nuclei around Pb is still considerable. Here we notice that the yields of transuranic nuclei is relatively higher than those in central collisions, which is because the excitation energies of primary fragments are much lower than those in central collisions. For peripheral collisions (see Fig.10(c) and (d)), elastic or inelastic scattering play a dominant role and the behavior of low energy fission of actinide nuclei is shown. The small shoulder around Pb seems to appear for impact parameters $b=8-10\text{fm}$ (see Fig.10(c)).

In order to make comparison with experimental measurement we have to make selection of scattering angle to fit the angle cut in experimental data, i.e. only fragments with the scattering angles of $56^\circ \leq \theta \leq 84^\circ$ and $96^\circ \leq \theta \leq 124^\circ$ in the center of mass frame are selected[9]. In the calculations, we assume that the scattering angle of residue of the primary fragment which undergoes emission of light charged particles is the same as the fragment itself. This assumption is roughly reasonable since the mass of residue is much larger than that of emitted light particles. For fragments from fission, we assume that the outgoing angle of one fragment is randomly distributed in the rest frame of the fissioning nucleus and the outgoing angle of the other one is then obtained by momentum conservation. Finally, we obtain the mass distribution of the final products with the same scattering angle cut as that in the experiment. The results are shown by open triangles in Fig.11. The experimental mass spectra from [9] are also indicated by solid squares, open squares, solid circles, open

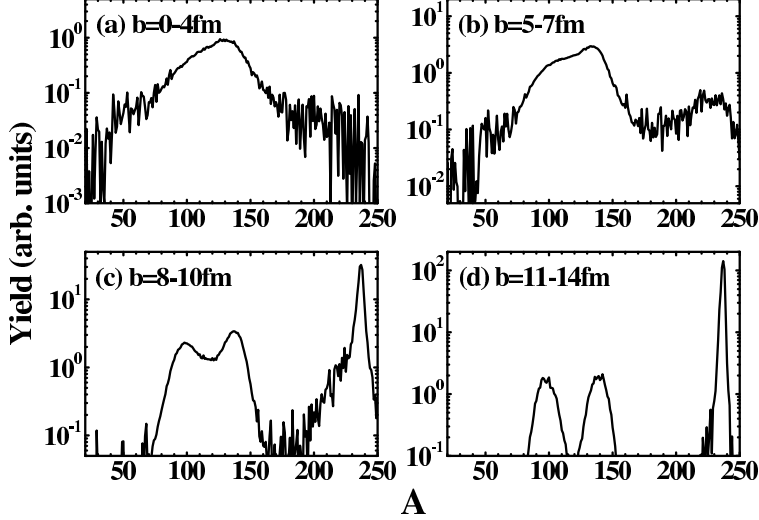


FIG. 10: The mass distribution of the products in $^{238}\text{U} + ^{238}\text{U}$ at different impact parameter regions.

circles and solid triangles for incident energies of 6.09, 6.49, 6.91, 7.10 and 7.35 AMeV, respectively, in Fig.11. From the figure we find that the behavior of the calculated mass distribution at 7.0 AMeV is generally in agreement with the data at incident energy 7.10 AMeV except the yields at mass region from 170 to 210 to be overestimated compared with experimental data. The following most important features of mass distribution can be deduced: (1) A dominant peak around uranium is observed, which can be attributed to the contribution of the reactions with large impact parameters seeing from Fig.10; (2) The step decreasing yield above U with the increase of the mass number is appeared. The products at this mass region stem from large mass transfer in small impact parameter reactions; (3) A small shoulder can be seen in the distribution of the products around Pb, compared with the products with mass near and smaller than Uranium for which the yields decrease exponentially as mass decreases. The appearing of small shoulder around Pb is due to the very high fission barrier around Pb. The central, semi-central collisions and even reactions with $b=8-10\text{fm}$ contribute to the shoulder around Pb region; (4) In the region below $A \approx 190$, the double bump distribution is observed. These products are from the fission of actinide and transuranium nuclei obviously, which are superposition of symmetric and asymmetric fission.

V. SUMMARY

In this paper, we apply the microscopic transport model, namely the ImQMD model

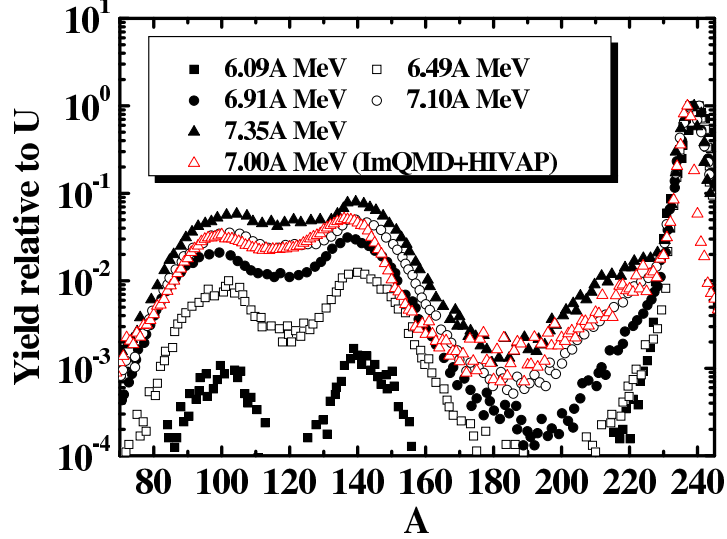


FIG. 11: (Color online) The mass distribution of the products of reaction $^{238}\text{U}+^{238}\text{U}$. The experimental data are from [9].

incorporating the statistical decay model and empirical three Gaussian fission model to study the reaction mechanism and the mass distribution of products in the reaction $^{238}\text{U}+^{238}\text{U}$ at the incident energy of 7.0 A MeV. The mass, charge and excitation energy distributions of primary fragments are calculated within the ImQMD model and the de-excitation process of those primary fragments is studied by using the statistical-evaporation model (HIVAP code). The impact parameter dependence of the mass distribution of primary fragments and final products are analyzed, from which the origin of products at different mass region can be understood. Finally, the mass distribution of final products in $^{238}\text{U}+^{238}\text{U}$ collisions with scattering angle cut is calculated in the first time and compared with recent experimental data. The main features of experimental mass distribution are reproduced, those are: (1) A dominant peak around the uranium nuclei is observed, which corresponds to elastic and quasi-elastic reaction products; (2) The yields of the transuranium nuclei decrease rapidly with increase of the mass A ; (3) A small shoulder can be seen in the mass distribution of the products around Pb on the background of products for which their yields decrease with their mass deviating from uranium exponentially. Those products are the residues of primary fragments surviving from multiple-particle evaporation; (4) In the region below $A \approx 200$, the double hump mass distribution is observed, which are the fission products from superposition of symmetric and asymmetric fission and mainly come from the fission of nuclei around uranium and transuranium fragments at high and low excitation energies. The main

discrepancy of our calculated results with experimental data is overestimate of mass yields in region of 170-200 and underestimate of mass yield of transuranium nuclei, which mainly come from the calculation of fission mass distribution for actinide and transuranium nuclei and fission width at high excitation energies. Further study is still under a way.

ACKNOWLEDGMENTS

This work is supported by the National Natural Science Foundation of China Nos. 10675172, 10875031, National Basic Research Program of China No.2007CB209900.

-
- [1] K.D.Hildenbrand, H.Freiesleben, F.Pühlhofer, et al., Phys.Rev.Lett.**39**, 1065(1977).
 - [2] M.Schadel, J.V.Kratz, H.Ahrens, et al., Phys.Rev.Lett.**41**, 469(1978).
 - [3] H.Freiesleben, K.D.Hildenbrand, F.Pühlhofer, et al., Z.Physik **A 292**, 171(1979).
 - [4] V.I.Zagrebaev and W.Greiner, J.Phys.G: Nucl.Part.Phys.**34**,1(2007).
 - [5] V.I.Zagrebaev, Yu.Ts. Oganessian, M. G. Itkis and W.Greiner, Phys. Rev. **C 73**, 031602(R) (2006).
 - [6] Ning Wang, Zhuxia Li, Xizhen Wu, et al., Mod.Phys.Lett.**A 20**,2619(2005).
 - [7] Junlong Tian, Xizhen Wu, Kai Zhao, Yingxun Zhang, Zhuxia Li, Phys. ReV. **C 77** 064603 (2008).
 - [8] Cédric Golabek and Cédric Simenel, Phys. Rev. Lett. **103**, 042701 (2009);
Cédric Simenel and Benoît Avez, Cédric Golabek, arXiv: 0904.2653V1 [nucl-th] 17 Apr. 2009;
 - [9] C.Golabek, A.C.C.Villari, S.Heinz, et al., Int.J.Mod.Phys.**E 17**, 2235(2008).
 - [10] S.Heinz, W.Mittig, A.C.C.Villari, et al., GSI Sci.Rep,p.136,2006; S.Heinz, C.Golabek, W.Mittig, et al., GSI Sci.Rep,p.147,2007
 - [11] Ning Wang, Zhuxia Li and Xizhen Wu, Phys. Rev. **C 65**, 064608 (2002).
 - [12] Ning Wang, Zhuxia Li, Xizhen. Wu,*et al.*, Phys. Rev. **C 69**, 034608 (2004).
 - [13] J. Cugnon, D. L'Hôte, and J. Vandermeulen, Nucl. Instrum. Methods Phys. Res. **B111**, 215 (1996)
 - [14] Yingxun Zhang, Zhuxia Li, Phys. Rev. **C 74**, 014602 (2006).
 - [15] Qingfeng Li and Zhuxia Li, Phys. Rev. **C 64**, 064612 (2001).
 - [16] W.Reisdorf, F. P. Hessberger, K.D. Hildenbrand, et al., Nucl. Phys. A **444**, 154(1985).

- [17] E.F.Neuzil and A.W. Fairhall, Phys.Rev.**129**, 2705(1963).
- [18] J.Benlliure, A.Grewe, M.de Jong, et al., Nucl.Phys.**A 628**, 458(1998).
- [19] K.-H.Schmidt, S.Steinhäuser, C.Böckstiegel, et al., Nucl.Phys.**A 665**, 221(2000).
- [20] D.M.Gorodisskiy, S.I.Mulgin, V.N.Okolovich, et al., Phys.Lett.**B 548**, 45(2002).
- [21] IAEA Library Cataloguing in Publication Data, Fission Product Yield Data for the Transmutation of Minor Actinide Nuclear Waste, international Atomic Energy Agency, Vienna, (ISBN 92-0-115306-6), 2008.
- [22] L. E. Glendenin, J. E. Gindler, I. Akmad, et. al., Phys. Rev.**C 22**, 152 (1980).
- [23] H. W. Schmitt, W. E. Kiker and C. W. Williams, Phys. Rev. **137**, B837 (1965).
- [24] W. John, E. K. Hulet, R. W. Lougheed, and et. al.,Phys. Rev. Lett.**27**,45 (1971).